Deep oxidation of aluminum by a DC oxygen plasma

J.A. Baier-Saip[a,*], J.I. Avila[a], G. Tarrach[a], A.L. Cabrera[a], V. Fuenzalida[b], R.A. Zarate[b,1], I.K. Schuller[c]

[a]*Facultad de Fisica, Pontificia Universidad Catolica de Chile, Casilla 306, Santiago 22, Chile*
[b]*Facultad de Ciencias Fisicas y Matematicas, Universidad de Chile, Av. Blanco Encalada 2008, Santiago 6511226, Chile*
[c]*Physics Department, University of California - San Diego, La Jolla, CA 92093-0319, United States*

Abstract

A novel way of oxidising aluminum using a DC oxygen plasma is described. The oxidation is carried out with a pressure of ~0.1 bar, an electrical current lower than 3 mA, and a working distance between the electrodes of the order of 1 cm. The pressure is seen to have a stronger influence on the results than the working distance. The process does not damage the surface and only minor differences are detected in the topography due to the expansion of the aluminum during oxidation. It is shown that the region affected by the plasma results in a ~50-nm-thick amorphous aluminum oxide layer (OL). We find that the kinetics of oxide growth can be described as having two main sources, the main one originating from the plasma and the other from the surrounding ionized gas.

Keywords: [B] Amorphous; [B] AFM; [B] SEM; [B] AES; [B] Raman scattering spectroscopy; [D] Aluminum oxide

1. Introduction

Metal oxides including ultra thin epitaxial oxide films play an important role in materials research, displaying metallike, semiconductorlike, and insulatorlike properties [1]. In particular, the behavior under very high tunneling current is of significant interest in microelectronics [2]. The alumina plays an important role here because of its large dielectric constant (~10), large barrier height for electron tunnelling (~2 eV), high corrosion resistance, good thermal and mechanical stability, and good adhesion [3–6]. The salient features of aluminum oxide make it also interesting for many potential technological applications [7–10].

There has been an increasing interest to grow alumina films in magnetic tunnel junction devices [11–14], which find applications as magnetic sensors and nonvolatile memories. In the magnetic tunnel resistance effect, the Al_2O_3 works as a barrier-insulating material and in order to avoid electrical conductivity the surface must be free from defects, i.e., barrier pinholes [15]. This effect is extremely sensitive to the precise interface structure [16,17], and the usual way to prepare such thin oxide films is to evaporate an aluminum layer and subsequently oxidise it.

Oxidation of aluminum up to 2 nm is a straightforward process [18], but deeper oxidations are difficult to produce since the initial layer shields further oxidation. In the last decade, attention has been given to the study of the initial oxidation stages [19], as these were not well understood and are still a subject of research [20]. On the other hand, the latest stage of oxidation is well described by the Cabrera–Mott theory [21,22].

The main focus of this work is to produce thicker alumina layers than those employed in microelectronics. Although very thick layers (tens of micrometers) may be produced by electrochemical methods, from a microscopic point of view, the resulting surface presents many defects, e.g., in the form of hexagonal channels. The proposed technique offers the possibility of improving surface flatness

* Corresponding author. Tel.: +56 2 3547152; fax: +56 2 5536468.
E-mail address: jbaier@fis.puc.cl (J.A. Baier-Saip).
[1] Present address: Universidad Catolica del Norte.

and purity, keeping it free from contaminants such as acids present in electrochemical solutions.

Low pressure plasmas are indispensable for advanced materials processing in many high technology industries [23]. In this paper, we address the problem of deep oxidation by implementing a new technique which makes use of a continuous high pressure oxygen plasma. The next section describes the experimental setup as well as several techniques used to characterize the oxidised samples. Following that, we present the measurements and then discuss the results. Finally, we summarize our conclusions and point out perspectives for future work.

2. Experimental

2.1. Sample oxidation

The basic experimental setup is shown in Fig. 1a. Aluminum samples with sizes of 1.72 $cm^2 \times 0.013$ cm thick were cut from a high purity Al foil (99.997%) from Alfa Aeasar. The process requires no special treatment of the surface before oxidation, and the surface has been cleaned by standard methods using an ultrasonic bath with methanol. The sample is placed in oxygen atmosphere whose pressure lies in the range from 50 to 100 Torr. Prior to oxygen exposure (99.8% pure oxygen, the main impurity is nitrogen), the chamber was outgased several times for periods of some hours.

Inside the chamber, the sample touches perpendicularly the electrode maintained at higher potential (hereafter referred to as the positive electrode), and the working distance to the electrode kept at lower potential (the negative electrode) was varied between 0.4 and 1.6 cm. The only metal pieces in the vicinity of the sample are the electrodes which are also made of high purity Al wire. The flowing

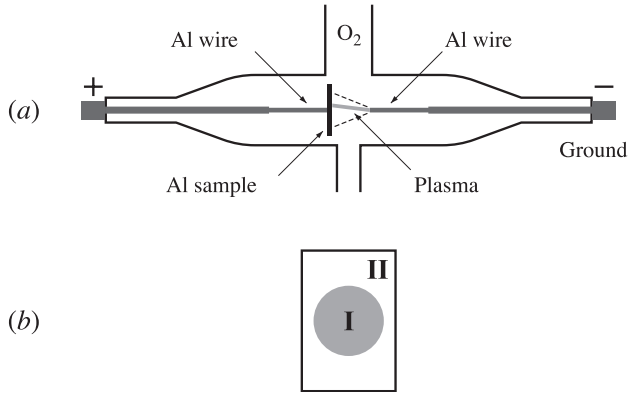

Fig. 1. (a) Experimental setup for oxidation. The positive electrode touches the Al sample and the negative electrode has a sharp tip. The plasma beam originates at the negative electrode and is confined to move within the region limited by the broken lines. (b) Cross-section view of the Al sample after oxidation. The region I (represented as a gray circle) is affected by the plasma and it presents a weak blue color, which is similar to that obtained when oxidising aluminum by electrochemicals methods (deep blue color).

electrical current is less than 3 mA and remains constant during the experiment. The voltage across the electrodes is around 500 V, and the precise value depends mainly on the oxygen pressure. As the oxidation progress, the voltage shows small variations because the oxide layer (OL) thickness grows and the electrical resistance increases.

2.2. Plasma characterization

The plasma diagnostic was performed with the Ocean Optics PC2000 Plug-in Spectrometer using the optic fiber QP50-2-VIS/NIR and the slave channel 1 for measurements in the spectral range from 340 to 1030 nm. The spectrometer was operated in the time acquisition mode, and the resulting spectrum is the average of 5 spectra with an integration time of 5 s for each spectrum.

2.3. Electron microscope images

Images from the surface revealing the topography of the sample were taken using a scanning electron microscope (SEM) from LEO Electron Microscopy, model 1400 VP. It was operated in the high vacuum mode (~10^{-6} mbar), with 10 keV electrons, 100 μA beam current, and a working distance of 6 mm. The secondary electron detector had a collector bias voltage of 370 V. Since alumina is an insulator, the samples have been coated with gold in order to avoid charging effects and to improve the resolution.

2.4. Atomic force microscope

The atomic force microscope (AFM) is a home-built microscope head operated by an RHK STM-100 electronics. Normal force and lateral force are measured by means of laser beam deflection with a four-quadrant photodiode. The presented images were obtained in contact mode with a standard cantilever of 0.1 N/m elastic constant. However, a 20-nm-thin gold coating had been applied to its backside in order to achieve better reflectivity. The estimated total repulsive force was less than 1 nN. A single-tube scanner with a maximum range of 11 μm has been used. Images were acquired with 256 points×256 lines and 0.52 s/line each way.

In particular, the RMS roughness was calculated by finding first the plane which best fits the measured data $z(x,y)$ and subtracting the plane from the original data. With this operation, the average height is set equal to zero and any inclination of the samples along the x and y axes is eliminated. Then the RMS value is obtained from these data by standard methods taking zero as the mean value.

2.5. Cross-section profiles

Surface cleanliness of the foils was monitored with Auger electron spectroscopy (AES) in an independent vacuum chamber with a base pressure better than 1×10^{-9}

Torr. The AES analyses were performed with a spherical mirror analyzer from Physical Electronics using 3 keV electrons and a 50 nA beam current [24,25]. The spectra were obtained in the energy range 50 to 1400 eV. The intensity N (number of electron counts/second) was measured as function of energy E, and then the derivative dN/dE was calculated around 68, 504, and 1382 eV to obtain the characteristic peaks of Al, O, and Al_2O_3, respectively. The Auger spectrum is affected in insulators [26], but the measured peak position energies are in good agreement with standard values. Since the total number of electron counts/second does not remain constant, the spectra have been normalized according to the initial value. Furthermore, when the derivative becomes very low and only noise is observed in the spectrum, the corresponding peak has been set equal to zero.

AES measurements were also conducted to characterize the sample after oxidation. In order to obtain an AES profile, Ar ions with 4 keV energy and a 0.5 μA beam current were used to erode ~0.05 cm^2 of the oxidised surface. The Ar ion gun was aligned at 60 from the surface normal. A previous calibration with a 100 nm SiO_2 layer resulted in an erosion rate equal to 4×10^3 nm/(C cm^{-2}), and with the present experimental parameters, it would correspond to 2.4 nm/min. The relative hardiness of Al_2O_3 and quartz is 2800/1250=2.24 [27]; hence, we expect a rate ~1.1 nm/min for the oxidised Al samples.

2.6. Raman

Raman spectroscopy was performed with a LabRam 010 instrument from ISA using 5.5 mW of a 632.8 nm HeNe laser. The Raman microscope was operated in a back-scattering geometry, where the incident beam is linearly polarized and the spectral detection is unpolarized. We used an Olympus MPlan 100× objective lens (numerical aperture NA=0.90), and the high NA indicates that depolarization effects must be expected [28].

2.7. Charge and area measurements

The total charge which flows during the experiment was calculated by integrating the electrical current read from a Keithley multitester model 177 μV DMM. The region of the sample impinged on directly by the plasma can be distinguished optically after the experiment; its area, hereafter named S_I (see Fig. 1b), is evaluated from the data acquired by scanning the surface.

3. Results

The identification of the lines present in the plasma spectrum can be obtained from the NIST database and from the literature [29]. The spectrum contains the characteristic lines of single ionized monoatomic oxygen O^-; the lines of O_2^+ are also present, but the corresponding intensity is much lower. The spectrum does not show any significative variation when changing parameters such as gas pressure and electrode distance within the range specified in our experimental conditions.

In above experiment of plasma oxidation, the plasma is mainly formed by negative oxygen ions travelling from the negative to the positive electrode. The positive molecular oxygens move in the opposite direction and they do not reach the sample; that is, they give no contribution to the oxidation. The beam has a diameter of ~1 mm which is approximately the same diameter as the electrode. The plasma slowly scans the sample surface contained within the cone delimited by the shadow lines as shown in Fig. 1a.

Two main characteristic regions of the sample can be distinguished after oxidation (Fig. 1b). We label I the region affected directly by the plasma flux, whereas II is the region impinged on only by ions coming from outside the plasma. Region I is shaped in a disc and increases with time as the plasma scans the surface.

In order to verify how the plasma affects the surface, SEM images were taken before oxidation of the sample and after oxidation in region I (Fig. 2). No damage to the surface is observed demonstrating that the plasma oxidation process is nondestructive. The topography before oxidation reveals a series of parallel lines with separations in the submicrometer range. Such lines are typical of metal sheets which have been fabricated by extrusion.

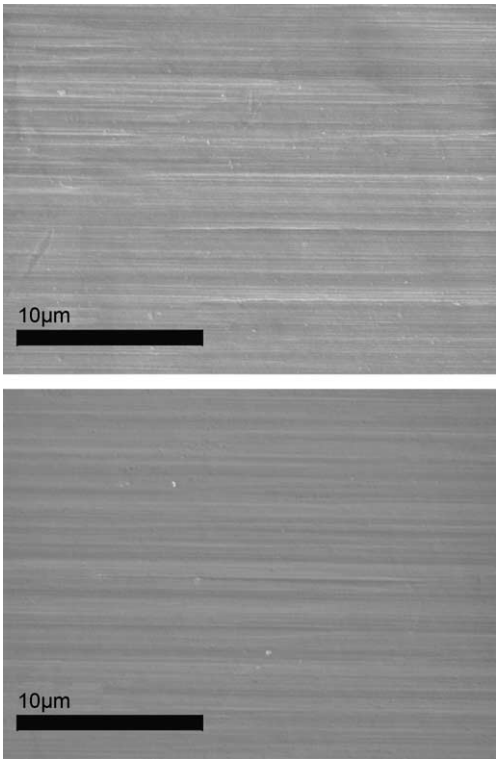

Fig. 2. SEM images of the sample before oxidation (top) and after oxidation in region I (bottom).

A closer look to see how the plasma modifies the surface is given by the AFM images. The RMS roughness before oxidation (Fig. 3a) and after oxidation (Fig. 3b) are equal to 12.4 and 10.4 nm, respectively. Although these values show small variations when measuring different sample locations, the roughness is always smaller in oxidised samples.

AES profiles were performed in order to get concrete proof of the existence of alumina and to investigate the OL thickness (Fig. 4), which is proportional to the erosion time needed to decrease the Al_2O_3 signal to half of its maximum value. Thus, as seen in Fig. 4, the region which suffers the largest oxidation is that impinged on by the plasma.

It has not been possible to obtain the atomic percent value directly by measuring the relative Auger peak intensities because the sensitivity factors are given for cylindrical mirror analyzers and not for spherical ones. However, since only the characteristic peaks of Al_2O_3 have been detected inside the OL with no traces of metallic aluminum, Al^+ or Al^{2+}, the average intensity of Al_2O_3 has been set to 100% of the atomic percent value and the corresponding intensity of oxygen to 60%. The same procedure was followed for aluminum inside the bulk. Furthermore, it can be concluded that a stoichiometric formation of Al_2O_3 appears [30].

The aluminum foil not oxidised in the chamber contains only a native OL characteristic of surfaces exposed to atmospheric pressures for long times. The corresponding AES profile (Fig. 4d) shows the smallest thickness and, from this graph, we can estimate the correlation of depth with the erosion time. The width at half height is 2 min, which corresponds to the native OL thickness of about 2 nm. Since it takes 2 min to erode 2 nm of the native OL, it follows that 1 min of erosion digs approximately 1 nm in the alumina under the defined experimental conditions. This result is consistent with the erosion data of hard materials measured with other experimental techniques. The largest oxidation depth shown in Fig. 4a is then ~50 nm, more than 20 times the native OL thickness. The presence of native oxide can then be considered insignificant with no influence on the oxidation produced by the plasma.

Fig. 5 shows the Raman spectra of the sample after oxidation. No characteristic Raman peak of crystalline alumina but only a broad luminescence line centered at 2000 cm^{-1} is obtained for region I, and region II presents the same behavior but exhibiting a lower degree of intensity. Further in region I, two weak Raman peaks appear at frequencies of 1300 and 1600 cm^{-1}, and they are similar to those in the spectrum of graphite. Carbon was detected by AES at the surface of the OL, but this has not been included in Fig. 4 for the sake of simplicity.

The total charge q which flows during the experiment was measured since the charge is proportional to the number of oxygen ions which strike the surface. Consequently, the amount of Al_2O_3 is expected to increase with the charge. The influence of pressure and the electrode to sample distance on oxidation was investigated by varying the parameters by a factor 2 and 4, respectively. Results are

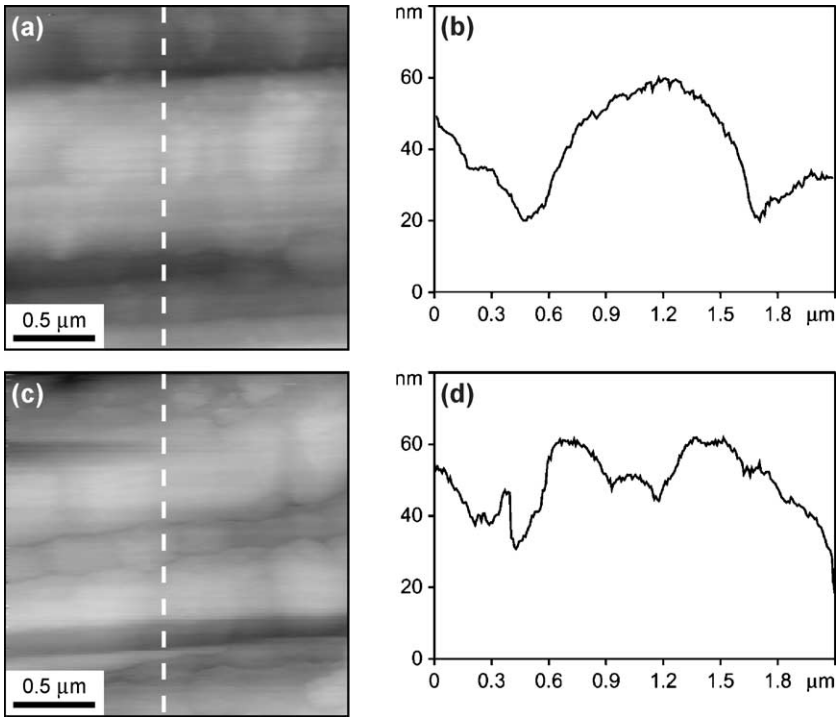

Fig. 3. AFM images of the sample (a) before and (c) after oxidation. The gray scale is same in both images and corresponds to the 80 nm of the cross-section. A cross-sectional view corresponding to the vertical dashed line (y axis) is displayed to the right of each image. The bottom of each line corresponds to y=0 μm and the top to y=2.1 µm. No cross-section along the horizontal x axis is given since it displays much smaller variations.

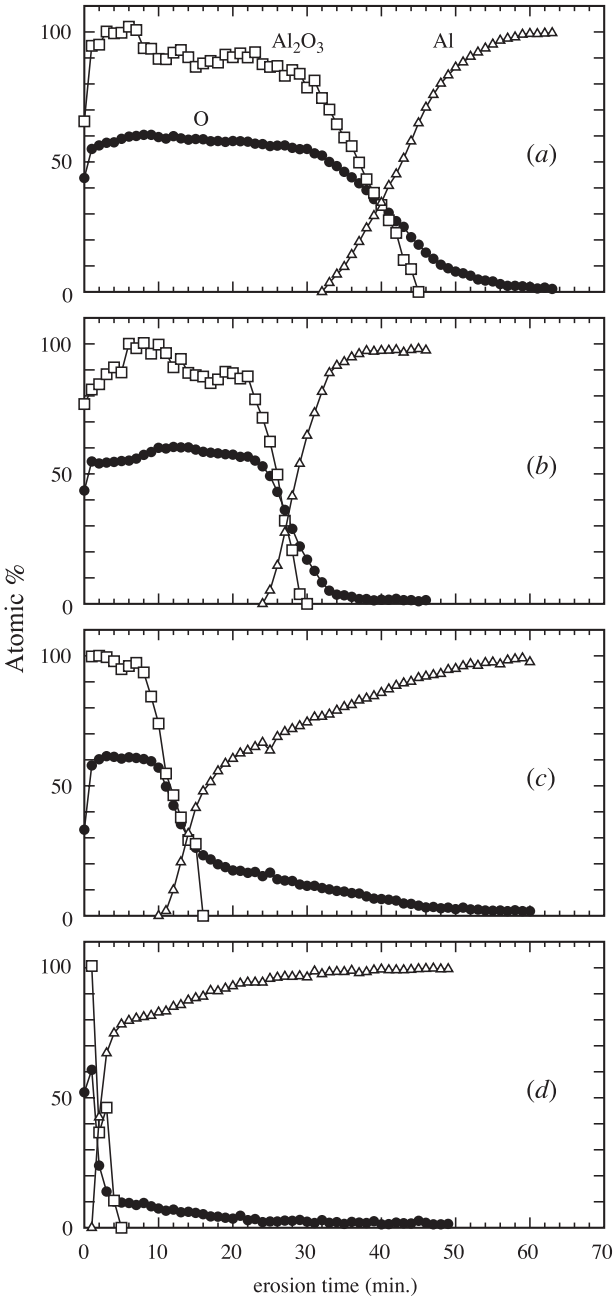

Fig. 4. AES profiles of the regions (a) I=at the center, (b) I=displaced from the center, and (c) II. A spectrum of an aluminum sample having only the native OL has been included in (d) for reference. The depth is proportional to the erosion time and estimated as 1 nm/min in the text.

summarized in Tables 1 and 2 and include the recorded total oxidation time and the area of region I.

4. Discussion

During oxidation, once a thick OL is formed by the plasma beam over a point at the surface, negative charges start to accumulate because the Al_2O_3 is a highly ionic material with a low electrical conductivity. The plasma is

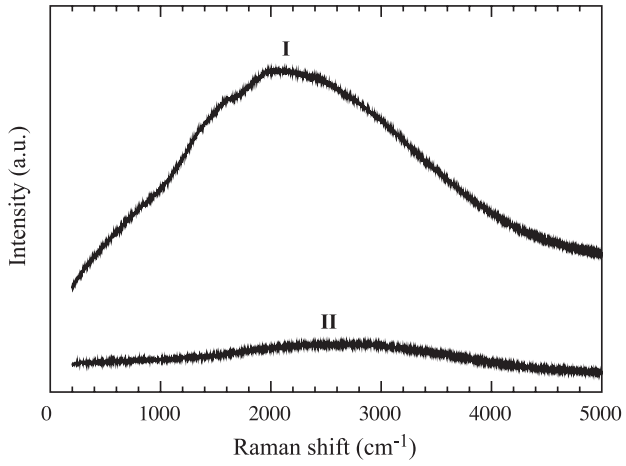

Fig. 5. Raman spectra of regions I and II of an oxidised aluminum sample. Except for the weak lines at 1300 and 1600 cm^{-1}, no Raman spectra but only a luminescence line centered at 2000 cm^{-1} is observed.

then deviated by the electric field generated by this charge so that it impinges upon a new location. The typical movement of the beam over the surface is spirallike, starting at the center where the electric field between the sample and the electrode is stronger at the beginning. Since the topography corrugation decreases and aluminum expands ~30% upon oxidation, this seems to indicate that the valleys suffer larger oxidations than the tips mainly because more oxygen ions are adsorbed in the valleys.

The oxidation does not solely arise from the ions forming the plasma. Some oxygen ions generated outside the plasma are constantly impinging on the sample surface slowly growing an OL. This builds at later stages an insulating OL which is thick enough to accumulate a negative charge, hindering the plasma from reaching the surface as explained previously. The plasma then bypasses the sample; that is, it is deviated to the positive electrode and the oxidation process stops.

The usual mechanism by which a metal is oxidised, according to the Cabrera–Mott theory, is by ion transport across the OL. Usually, either the metallic ion or the oxygen ion moves, and it has been found that in the specific case of alumina, the Al ions move to the surface [22,31]. The dominant defects within the oxide which contribute to ion

Table 1
Total charge q for different electrode separations D at constant pressure of 70 Torr

D (cm)	S_I (cm^2)	t (min)	q (C)	q_D (C)	Difference (%)
0.4	0.414	22	3.60	3.62	+0.6
0.6	0.375	21	3.39	3.42	+0.9
0.8	0.637	48	7.66	7.44	−2.9
1.0	0.641	47	7.28	7.31	+0.4
1.2	0.871	42	7.12	7.04	−1.1
1.4	0.641	36	5.77	5.86	+1.6
1.6	0.992	72	11.11	11.22	+1.0

The area S_I of the region affected by the plasma and the oxidation time t are also given. The charge q_D is calculated using Eq. (1) and the difference between theoretical and experimental values is displayed in the last column.

Table 2
Same as in Table 1 but now the oxygen pressure P changes and the electrode separation is kept constant at 1.0 cm

P (Torr)	S_I (cm^2)	t (min)	q (C)	q_P (C)	Difference (%)
50	0.609	29	4.53	4.78	+5.5
60	0.668	45	7.47	7.21	−3.5
70	0.641	47	7.28	7.48	+2.7
80	0.676	35	6.01	5.73	−4.7
90	0.625	21	3.57	3.60	+0.8
100	0.465	31	4.83	4.97	+2.9

The charge q_P is calculated using the same equation but with new fitted parameters.

transport are metal vacancies and the rate-determining reaction occurs at the oxide film/gas interface. At the interface between the positive metallic ion and the ionized absorbed oxygen exists a constant contact potential, which generates a large electric field ~10^9 V/m for very small separations, i.e., thin OL [21]. This is the main driving force which acts over the ions forcing them to diffuse. The field intensity is such that space charge effects become negligible and the diffusion of ions induced by concentration gradients is very weak.

The relatively smooth transition between the oxide and the metal seen in the AES profiles can be explained if we recall that during argon ion bombardment a small fraction of the extracted oxygen forming the alumina does not fly away, but is deposited near the center of the generated hole. Consequently, small contaminations from upper levels occur during erosion, and since AES is particularly sensitive to oxygen, a weak signal indicating the presence of oxygen is obtained where it did not originally exist. Such pseudo-smooth transitions are typical in AES profiles specially when the substrate is soft such as aluminum. As usual, we assume the boundary to be the point where the peak intensity is equal to half its maximum value, and we do not take further the transition region into consideration.

Let us now analyze the OL thickness formed over the different regions. We recall that the plasma covers region I, and the ionized gas falls over regions I and II. The largest thickness occurs in the center of region I and decreases away from it. In order to explain this result, we consider the energy of the ions and the intensity of the electric field in the surface of the sample. Since kinetic energy is dissipated by viscous flow, the energy of the ions falling far from the center of region I is smaller because they rove a larger distance. It has been shown that the sticking coefficient increases with the kinetic energy of the incoming O_2 molecule [32]. As a result, the plasma induces a deeper oxidation near the center because more oxygen atoms are adsorbed and the electric field is stronger in this point.

The intensity of inelastic light scattering depends on the interaction volume, and, in the present case, it is proportional to the OL thickness. For layers much smaller than the wavelength of the laser, the luminescence and the Raman effect are very weak. This is consistent with the fact that the OL in region II is thinner than in region I as confirmed by the Auger profile measurements.

Luminescence is characteristic of solids such as insulators [33] and alumina belongs to this category. This effect is enhanced if there exists a large concentration of point defects in the sample, e.g., if it is amorphous. On the other hand, the Raman effect is visible when there exists long range order in the solid. The strong luminescence in our samples makes impossible the observation of Raman lines [34], and this indicates that no crystalline but rather an amorphous phase was formed. When oxidising aluminum a ã-amorphous phase is generally formed [1,35], but it can be changed into an á-crystalline phase upon annealing at 1200 °C for about 30 min [36].

It is not a simple task to obtain quantitative information relating the OL formation to the oxidation conditions by making AES profile measurements at different points for each sample, since the amount of data required is huge and the surface near each point is destroyed during the measurement. A more straightforward and practical way is to measure a plasma property which can be connected with the oxidation. As pointed out in the previous section, the amount of alumina increases with the total charge which flows during the experiment. We will see next that the amount of charge can provide qualitative information.

The total charge can be separated into two parts (see Fig. 6). One part q_p appears in the form of a plasma and the other q_g as a scarcely ionized gas or free electrons which are not bound to ions. Firstly, we assume that for fixed parameters (e.g., constant pressure and voltage), the plasma deposits a uniform amount of oxygen ions per unit area as it scans the surface. This is only an approximation and it is supported by fact that the scanning is continuous and well behaved. Thus, a constant charge density σ_p is produced over region I, and $q_p=\sigma_p S_I$, where S_I is the area affected by the plasma.

It is also assumed that the ionized gas falls uniformly over the whole surface, increasing the amount of oxygen ions deposited. For a constant ion flow, the latter is proportional to the total oxidation time t, and $q_g=i_g t$, where i_g is the current associated with the ionized gas and

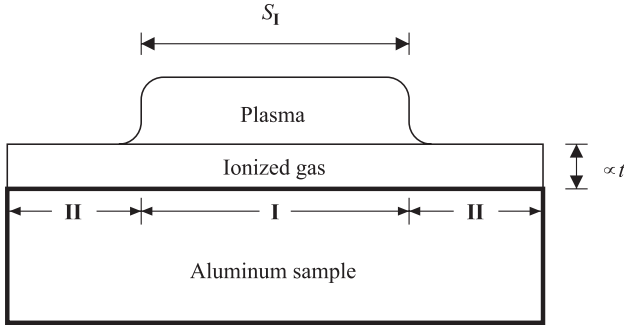

Fig. 6. Cross-section view of oxygen deposited over the sample during experiment. The amount of oxygen deposited over region I by the plasma is proportional to the area S_I, and the amount of oxygen deposited over regions I and II by the ionized gas increases with time t.

the free electrons. The sum of the two charges yields the total charge

$$q = \sigma_p S_I + i_g t \quad (1)$$

Tables 1 and 2 present the calculated values for the charge q_D (varying distance) and for q_P (varying pressure) based on Eq. (1). In the first case, the parameters fitted by least square deviation are σ_{pD}=1.70 C/cm^2, i_{gD}=0.132 C/min=2.21 mA,[2] while in the second case, σ_{pP}=0.77 C/cm^2, i_{gP}=0.149 C/min=2.48 mA.[3] The corresponding RMS deviation for the first data set is χ_D=1.4% and for the second one χ_P=3.7%. It is also possible to fit both data together (varying distance and pressure) with σ_{pD+P}=1.17 C/cm^2, i_{gD+P}=0.141 C/min=2.36 mA, and in this case χ_{D+P}=3.1%. Since $\chi_D<\chi_{D+P}<\chi_P$, it can be concluded that the fit works well for the data set with variable distance and poorly for the data set with variable pressure; that is, in this simple form, Eq. (1) holds for distance variations but not for pressure variations.

One way to correct this deficiency is to let the parameters σ_p and i_g be functions of pressure. Since the relative variation in σ_p is much larger than i_g we assume the first to be pressure dependent and the second to be nearly constant. The value $i_g=i_{gD}$ obtained above represents about 80% of the total current. Furthermore, for P=70 Torr we have $\sigma_p=\sigma_{pD}$ and for other pressures σ_p can be determined by analogous measurements where the distance is varied and the pressure is kept constant at the desired value.

Because σ_p is related to the charge of ions coming from the plasma, it can be concluded that the amount of oxygen deposited by the plasma over region I is pressure dependent. This result is not unexpected since in a plasma the ionization produced by the electric current depends on the gas pressure. Varying the pressure modifies the particle density and the Debye length [37], i.e., the plasma properties, mainly affecting σ_p.

We now compare the charge densities over regions I and II. The charge density coming from the ionized gas is $\sigma_g=q_g/S_{I+II}=i_g t/S_{I+II}$, where S_{I+II}=1.72 cm^2 is the total sample area. For the oxidation times listed in Table 1 and $i_g=i_{gD}$, the density σ_g varies between 1.62 and 5.54 C/cm^2. The total charge density in region I is $\sigma_I=\sigma_p+\sigma_g$ and in II is $\sigma_{II}=\sigma_g$ so that σ_{II}/σ_I lies between 0.488 and 0.765. This should be equal to the ratio OL thickness of II by that of I if the OL formed were simply proportional to the amount of oxygen ions striking the surface and there were no free electrons contribution to σ_g. Therefore, the ratio between the OL thickness of region II and region I is smaller than σ_{II}/σ_I. From the Auger measurements (Fig. 4), comparing the thickness of two different points in region I with that of region II yields the ratios 0.33 and 0.50, in agreement with the previous discussion.

[2] σ_{pD}=charge density affected by plasma when varying the distance; i_{gD}=electrical current affected by the ionized gas when varying the distance.

[3] Same as before but with varying pressure.

5. Conclusions

We have described in detail the oxidation of aluminum by a DC oxygen plasma. It was verified that the plasma produces deep oxidation of bulk aluminum samples with no damage to the surface. From AFM measurements, it could be seen that the valleys suffer larger oxidations than the tips.

The AES profiles revealed that the OL thickness is larger at the center of the region affected by the plasma and decreases when moving towards the borders of the region. The main factors leading to this result are believed to be the larger sticking coefficient and the larger electric field at the center. Within the OL, a homogeneous Al_2O_3 was formed having no metallic or partially oxidised aluminum.

In region I, only a luminescence spectrum is obtained and no characteristic Raman lines of alumina are seen, pointing out that the oxide formed is rather amorphous. In region II, a similar effect is seen but with a much lower intensity, confirming the formation of a thinner OL.

Finally, the kinetics of OL growth has been separated into two main contributions arising from the plasma and the ionized gas. The former gives a uniform OL thickness over region I which depends on pressure, while the latter adds a layer over both regions proportional to the oxidation time. The oxidation parameters appearing in Eq. (1) were found to be nearly independent on the electrode separation.

The technique developed seems appropriate for producing thick amorphous alumina layers. Methods producing a uniform plasma over the entire sample's surface have still to be developed, and the influence of other parameters, such as temperature and electrical current, on the oxidation remain to be studied. It would also be interesting to see how the oxidised area S_I and the total oxidation time change when using, in place of bulk samples, thin aluminum films or aluminum wedges deposited over nonoxidised substrates. This could indicate the range of applicability of Eq. (1) when considering other parameters. More detailed and quantitative information on the OL could be obtained with cross-sections transmission electron microscope images.

Acknowledgements

Funds from FONDECYT 1030642, MECESUP PUC0006, Fundacion Andes 10810-2, and the U.S. Department of Energy are greatly acknowledged. We thank Walter Garrido, Guerau B. Cabrera, and Jorge Gomez for the initial feasibility experiments they performed, Mario Favre for helping in some measurements, and Luis Altamirano for technical expertise. We are also grateful to R. Matelon for comments and suggestions.

References

[1] H.J. Freund, H. Kuhlenbeck, V. Staemmler, Rep. Prog. Phys. 59 (1996) 283.
[2] J.F. Verwij, J.H. Klootwijk, Microelectron. J. 27 (1996) 611.
[3] M. Sharma, S.X. Wang, J.H. Nickel, Phys. Rev. Lett. 82 (1999) 616.
[4] T.W. Hickmott, J. Appl. Phys. 88 (2000) 2805.
[5] E.S. Snow, P.M. Campbell, R.W. Rendell, F.A. Buaot, D. Park, C.R.K. Marrian, R. Magno, Semicond. Sci. Technol. 13 (1998) A75.
[6] A.T.M. van Gogh, S.J. van der Molen, J.W.J. Kerssemakers, N.J. Koeman, R. Griessen, Appl. Phys. Lett. 77 (2000) 815.
[7] R.H. French, A.H. Heuer, J. Am. Ceram. Soc. 77 (1994) 292.
[8] L. Bideux, C. Robert, B. Gruzza, V. Matolin, Z. Benamara, Surf. Sci. 352 (1992) 407.
[9] N. Yoshimoto, T. Matsuoka, T. Sasaki, A. Katsui, Appl. Phys. Lett. 59 (1991) 2251.
[10] M.W. Finnis, J. Phys., Condens. Matter 8 (1996) 5811.
[11] J.M. Daughton, Thin Solid Films 216 (1992) 162.
[12] D.E. Heim, R.E. Fontana Jr., C. Tsang, V.S. Speriosu, B.A. Gurney, M.L. Willams, IEEE Trans. Magn. 30 (1994) 316.
[13] B.J. Jönsson-Åkerman, R. Escudero, C. Leighton, S. Kim, I.K. Schuller, D.A. Rabson, Appl. Phys. Lett. 77 (2000) 1870.
[14] B.F.P. Roos, P.A. Beck, S.O. Demokritov, B. Hillebrands, Surf. Sci. 497 (2002) L55.
[15] J.J. Åkerman, I.K. Schuller, J.M. Slaughter, R.W. Dave, Appl. Phys. Lett. 79 (2001) 1.
[16] J.S. Moodera, E.F. Gallagher, K. Robinson, J. Nowak, Appl. Phys. Lett. 70 (1997) 3050.
[17] Ph. Mavropoulos, N. Papanikolaou, P.H. Dederichs, Phys. Rev. Lett. 85 (2000) 1088.
[18] J.E. Crowell, J.G. Chen, J.T. Yates Jr., Surf. Sci. 165 (1986) 37.
[19] M. Schid, G. Leonardelli, R. Tscheließnig, A. Biedermann, P. Varga, Surf. Sci. 478 (2001) L355.
[20] A.J. Komrowski, J.Z. Sexton, A.C. Kummel, M. Binetti, O. Weiße, E. Hasselbrink, Phys. Rev. Lett. 87 (2001) 246103.
[21] N. Cabrera, N.F. Mott, Rep. Prog. Phys. 12 (1948) 163.
[22] T. Do, N.S. McIntyre, Surf. Sci. 440 (1999) 438.
[23] G.S. Oehrlein, Surf. Sci. 386 (1997) 222.
[24] A.L. Cabrera, J. Vac. Sci. Technol., A 8 (1990) 3229.
[25] A.L. Cabrera, J. Vac. Sci. Technol., A 11 (1993) 205.
[26] D. Briggs, M.P. Seah (Eds.), Practical Surface Analysis: Auger and X-Ray Photoelectron Spectroscopy, 2nd edition, John Wiley and Sons, New York, 1996.
[27] R.M. Brick, A.W. Pense, R.B. Gordon (Eds.), Structure and Properties of Engineering Materials, 4th edition, McGraw-Hill, New York, 1977, p. 431.
[28] G. Turrel, Practical Raman Spectroscopy, Springer Verlag, Berlin, 1989, Chapter 2, pp. 27–30.
[29] R.W.B. Pearse, A.G. Gaydon, The Identification of Molecular Spectra, 2nd edition, Chapman and Hall, London, 1950.
[30] Y. Wu, H.S. Tao, E. Garfunkel, T.E. Madey, N.D. Shinn, Surf. Sci. 336 (1995) 123.
[31] R. Jansen, B. Davis, C.T. Tanaka, J.S. Moodera, Surf. Sci. 463 (2000) 109.
[32] L. Österlund, I. Zorić, B. Kasemo, Phys. Rev., B 55 (1997) 15452.
[33] F. Williams, Luminescence of Inorganic Solids, Academic Press, New York, 1966, Chapter 1.
[34] T.J. Vickers, C.K. Mann, in: Chemical Analysis Series, vol. 114, John Wiley and Sons, New York, 1991, Chapter 5.
[35] P.J. Chen, M.L. Colaianni, J.T. Yates Jr., Phys. Rev., B 41 (1990) 8025.
[36] D.L. Cocke, E.D. Johnson, R.P. Merril, Catal. Rev., Sci. Eng. 26 (1984) 163.
[37] J.D. Jackson, Classical Electrodynamics, 2nd edition, John Wiley and Sons, New York, 1975, Chapter 10.